Bayesian Parameter Optimization to Improve Deep Brain Stimulation for Parkinson's Disease

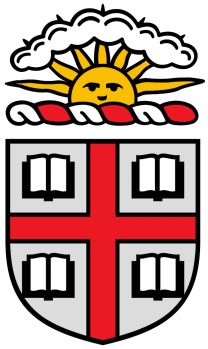

A thesis submitted in partial fulfillment of the requirements for the degree of Bachelor of Science with Honors in the Biophysics concentration at Brown University.

Ketan Pamurthy

Advisor: Shane Lee, PhD

Second Reader: Wael Asaad, MD, PhD

April 18, 2025

Table of Contents

Acknowledgements

I would first like to express my immense gratitude for all of the patients who participated in this research – none of this work would be possible without the time and energy that they so graciously volunteered. I also want to thank my advisor, Dr. Lee, for the opportunity to work on these amazing projects as well as the chance to share in his wealth of knowledge and passion for helping others through research. A special thanks also goes out to all of my friends and collaborators in the Computational Neuromodulation Lab, who helped me build intraoperative rigs, code behavioral tasks, and truly enjoy the last 2 years of research. Finally, I am eternally grateful for all of my friends and family who have been a constant source of encouragement and support.

Abstract

Parkinson's Disease (PD) is a degenerative neurological disorder characterized by motor dysfunction and linked to abnormal patterns of neural activity. Deep Brain Stimulation (DBS) has become a widely used treatment for its ability to disrupt pathological neural oscillations, yet traditional open-loop systems are limited by adverse side effects and an inability to adapt to real-time changes in symptom severity. Closed-loop DBS presents a promising alternative, recording live neural activity and tailoring stimulation to a patient's current pathological state. While most closed-loop approaches focus on adapting the timing of stimulation, fewer efforts have addressed optimization of the stimulation parameters themselves. In this study, we developed and tested a closed-loop framework for DBS parameter selection, using Bayesian optimization of the frequency and pulse-width of stimulation. To evaluate stimulation benefit, we targeted minimization of beta, spectral power in the 13–30 Hz frequency band, because of its well-established correlation to motor dysfunction in PD. We also developed a novel artifact rejection algorithm to remove stimulation artifacts from recorded local field potentials (LFPs), allowing for more accurate calculations of beta and other neural biomarkers. We showed that our artifact rejection algorithm successfully preserved temporal and spectral features of neural activity, in a way that is robust to long time scale fluctuations in the signal baseline. Additionally, we found that our Bayesian optimization method converged on low frequency/high pulse-width stimulation, highlighting the need for patient-specific parameter tuning. These results demonstrate the feasibility of using closed-loop optimization algorithms to target neural biomarkers and automate DBS parameter tuning.

Introduction

Overview of Parkinson's Disease

Parkinson's disease (PD) is a progressive neurodegenerative disorder that is commonly associated with cardinal motor symptoms including tremor, rigidity, slowness of movement (bradykinesia) and postural instability (Shahed et al., 2007). PD is the fastest growing neurological disorder in the world, projected to affect over 12 million people globally by 2040 (Dorsey et al., 2018). The most significant risk factor for PD is advanced age, although increased prevalence rates are also observed among males and people from developed countries (Willis et al., 2022; Zhu et al. 2024). The vast majority of PD cases (around 90%) are "sporadic," with no known definitive cause. However, many studies have linked increased risk to genetic susceptibility, along with environmental factors like chemical exposure and head trauma (Chade et al., 2006; Wood-Kaczmar et al., 2006).

PD is characterized by a progressive loss of dopamine-producing neurons in the substantia nigra pars compacta (SNpc), a midbrain structure of the basal ganglia. Cell death primarily occurs due to the presence of Lewy bodies, intraneuronal aggregates of the protein α-synuclein that disrupt normal cell function (Shults, 2006). Degeneration of SNpc neurons leads to dopamine depletion of the nigrostriatal pathway, a projection from the SNpc to the striatum (Sonne et al., 2024; Panicker et al., 2021). This decreased dopamine in the striatum causes dysregulation of the motor control pathways, resulting in the motor dysfunction seen in patients with PD.

In addition to the cardinal motor symptoms of PD, most patients experience one or more non-motor symptoms such as abnormal vision/smell, behavioral changes, autonomic dysfunction, sleep disturbances, or fatigue (Pfeiffer, 2016). Many of these symptoms are normal

side effects of aging, but PD patients have on average a greater number and higher severity of their non-motor symptoms. Assessment of these symptoms is typically conducted with the Unified Parkinson's Disease Rating Scale (UPDRS), a quantitative measure of both motor and non-motor symptoms (Ballard et al., 2009).

Current Treatments for PD

Although there is currently no cure for the progressive cell death underlying PD, there are several treatment options that can help patients manage their symptoms. The most effective and most common first-line therapy is levodopa, a dopamine precursor administered to replace the dopamine lost through degeneration of the SNpc (Buyan-Dent et al., 2018). Dopamine agonists, mono-amine oxidase (MAO) inhibitors, and catechol-*o*-methyltransferase (COMT) inhibitors can also be used to modify the dopamine metabolic pathway, maintaining high levels of striatal dopamine. Despite their clinical efficacy, however, these pharmacological treatments risk a variety of side effects such as headaches, nausea, vomiting, and hallucinations (Gandhi et al., 2023). Long-term use of levodopa can also result in dyskinesias (involuntary movements), greatly reducing its therapeutic window (Hansen et al., 2022).

Deep Brain Stimulation (DBS) has emerged as a transformative surgical treatment for PD, overcoming many of the limitations associated with pharmacological approaches. DBS involves surgical implantation of stimulating electrodes within target neural structures, such as the subthalamic nucleus (STN) or globus pallidus internus (GPi). Though the precise mechanism remains unknown, the therapeutic current administered through DBS electrodes modulates abnormal neural activity, alleviating motor symptoms. DBS has provided beneficial results for patients with medication-refractory PD, with advantages over other therapies due to its reversible

nature and the ability to adjust stimulation parameters to maximize benefit (Lozano et al., 2019). That said, DBS currently operates in an open-loop fashion, delivering continuous stimulation based on manually programmed settings. This paradigm does not account for real-time changes in neural activity or symptom severity, which makes it poorly suited for the dynamic nature of PD and can result in unwanted side effects (Rosin et al., 2011). Additionally, determination of the optimal stimulation parameters for each patient requires a time-intensive trial and error process that often must be repeated as the disease progresses.

Closed-Loop DBS

Closed-loop DBS is a strategy in which stimulation is delivered in response to the patient's real-time pathological state. In contrast to the fixed nature of traditional open-loop DBS, closed-loop DBS systems use recorded neural activity as feedback to dynamically adapt the timing and parameters of stimulation (Cuschieri et al., 2022). Although it is not yet the standard of care, closed-loop DBS has seen a rapid increase in clinical applications due to its ability to optimize treatment by reducing battery usage and avoiding side effects of overstimulation (Rosin et al., 2011).

Closed-loop DBS systems operate based on symptom-related biomarkers, tailoring stimulation to minimize those biomarkers in recorded neural signals. For example, beta power (oscillatory activity in the 13–30 Hz frequency band) has emerged as a key biomarker due to its strong correlation with rigidity and bradykinesia. Beta's role as a therapeutic target is also supported by the observation that both levodopa treatment and DBS result in a decrease in beta power, with the decrease from DBS being proportional to the amplitude of stimulation (Whitmer et al., 2012; Bouthour et al., 2019). Discovery of other symptom-specific and even

patient-specific biomarkers using machine learning methods is a major focus of ongoing research, increasing the potential of closed-loop DBS for highly personalized therapy (Scangos et al., 2021).

Parameter Optimization for DBS

For both open-loop and closed-loop DBS, the stimulation parameters which maximize benefit while minimizing side effects can be drastically different for each patient (Kuncel & Grill, 2004). As such, it is crucial to find a given patient's optimal frequency, pulse-width, amplitude, and electrode contact in an accurate and efficient manner. Traditional open-loop methods require manual iterative programming by a clinician along with a trial and error process which can be time-consuming and subjective. However, recent advances have explored the use of closed-loop systems and automated methods to find optimal DBS parameters more precisely, efficiently, and objectively.

One method common to several recent studies has been using imaging data from techniques like magnetic resonance imaging (MRI), functional MRI (fMRI), and diffusion tensor imaging (DTI) to build computational models for determining optimal parameters. For example, in a 2019 study conducted in patients undergoing DBS for essential tremor (ET), Vorwerk et al. found that their MRI and DTI-based finite element model predicted similar optimal electrode configurations to those determined clinically, in a fraction of the time required for clinical testing (Vorwerk et al., 2019). Similarly, a 2024 study by Qiu et al. found that a deep learning and fMRI-based method settled on similar optimal voltages, frequencies, and contact locations for PD patients compared to those determined through clinical optimization (Qiu et al., 2024). While these results do not establish algorithmically optimized parameters as providing improved

symptom relief compared to manually-determined settings, they establish that optimization strategies can produce comparable results with significantly greater efficiency.

Bayesian optimization is another strategy that several researchers have explored for parameter optimization in DBS, both through computational models and *in vivo* experiments. In a 2021 paper, Connolly et al. tested several algorithms *in silico* and determined that Bayesian optimization performed the best at maximizing cortical evoked potentials, a biomarker of symptom relief, and minimizing motor potentials, a biomarker of side effects (Connolly et al., 2021). Similarly, Grado et al. developed a Bayesian adaptive dual controller and demonstrated that it was superior to other optimization algorithms at efficiently minimizing beta power in a computational model of Parkinson's disease (Grado et al., 2018). Building on this computational work, Louie et al. applied Bayesian optimization methods in two patients with PD and showed that the algorithm could rapidly converge on optimal rigidity-reducing frequencies faster than manual or random tuning methods (Louie et al., 2021). A 2022 paper by Sarikhani et al. further highlighted the effectiveness of Bayesian optimization *in vivo*, demonstrating that their method's automatically determined stimulation amplitude and electrode contact produced comparable tremor suppression to clinically determined settings in patients with ET and PD (Sarikhani et al., 2022). These papers all show the potential of Bayesian optimization for automated parameter selection, highlighting the need for further studies that explore other biomarkers and evaluation metrics.

Stimulation Artifacts

A persistent challenge in the development and optimization of closed-loop DBS systems is the presence of stimulation artifacts, high-amplitude transients in recorded local field

potentials (LFPs). These artifacts arise from the electrical pulses delivered in DBS, due to simultaneous stimulation and recording from the same or nearby electrodes (Qian et al., 2017). Artifacts are typically several orders of magnitude larger than the underlying neural activity, which causes the generation of a strong spectral band at the stimulation frequency and its harmonics. This contamination in the frequency domain obscures relevant neural signatures and prevents accurate calculation of spectral biomarkers (like beta) that are important for adaptive DBS systems to evaluate stimulation effectiveness (Zhou et al., 2018).

Artifact rejection, the process of removing stimulation artifacts from LFPs, is therefore a critical component of achieving closed-loop DBS parameter optimization. Effective artifact rejection algorithms must preserve important neural information in the time and frequency domains, operate in real-time or highly efficiently, and adapt to variations in stimulation parameters and electrode configurations.

Research Goals

The goal of this study was to develop and test the performance of an experimental approach for automatically determining optimal DBS frequency and pulse-width, using a behavioral task to control the patient's neural state. We hypothesized that, through the use of Bayesian optimization strategies targeting beta power, our approach could efficiently and accurately determine the optimal frequency and pulse-width of stimulation for a patient. To ensure the accuracy of beta calculations, we also developed an artifact rejection algorithm that suppresses stimulation-induced distortions in LFP recordings.

Methods

Patient Data Collection

Patients recruited for this study were individuals undergoing awake DBS electrode implantation surgery as part of their clinical treatment for PD. Patients provided informed consent prior to the operation, and all research procedures were performed in accordance with an approved Rhode Island Hospital human research protocol (Lifespan IRB protocol #263157).

Electrode implantation was conducted based on standard stereotactic neurosurgical techniques, utilizing tungsten microelectrodes to record neurophysiological data and MRI/CT imaging to guide electrode trajectories. Patients are lying supine with the microdrives mounted onto a customized, 3D printed StaRFix platform. Typical targets for electrode placement were STN and GPi, depending on the patient's clinical presentation and evaluated in a comprehensive, multi-disciplinary clinic (Akbar & Asaad, 2017). Typical microelectrode arrays included the center, posterior, and lateral trajectories of a Ben-Gun array, depending on the planned trajectory. Microelectrode arrays were advanced along the preoperatively-determined trajectory to capture broadband multi-unit and single neuron spiking activity while ensuring minimal tissue disruption. After mapping of the trajectory based on microelectrode recordings, DBS electrodes (either Medtronic 3387/3389 or 33005/33015 directional leads) were implanted, and clinical stimulation parameter testing was performed. Patients remained awake throughout the operation to allow for real-time assessment of neural recordings and monitoring of both passive and active motor responses.

Our research experiments were performed following trajectory mapping and clinical parameter testing. Patients were instructed to engage in a pen and tablet-based behavioral task, during which recordings from the hemisphere opposite the patient's dominant hand were

collected from the neurophysiology data acquisition system (Alpha Omega, Nazareth, Israel) and transmitted via ethernet to a standard desktop computer which ran the Bayesian optimization algorithm. Stimulation was delivered to the most distal contact, Contact 0, of the DBS electrode, and optimization was performed based on the value of beta calculated from Contact 1a recordings, sampled at 44 kHz.

Behavioral Task

The behavioral task that patients followed was a modified version of the instructed-delay center out task with 8 targets (Tzagarakis et al., 2010). We chose this task with the goal of maintaining consistent levels of baseline beta power throughout the experiment, to make accurate comparisons between stimulation parameters. After an extensive literature review, we found that the "cue period" of the task outlined in this paper demonstrated relatively low variance in beta power compared to other cursor-based behavioral tasks.

Our modified task was performed as follows. The patient holds their cursor over a central fixation point for 500 ms, which triggers the appearance of 8 unfilled circular targets, 15 degrees counterclockwise from the cardinal directions. After the unfilled targets appear, the patient continues to hold their fixation within a small radius of the central point for 2 seconds, preparing for movement. During the first 1.5 seconds of this movement-preparation stage, the patient receives continuous stimulation from the macroelectrode contact, with parameters determined by the Bayesian Optimization algorithm. After the 2 second holding period is complete, one of the 8 circles becomes a filled target. Finally, the patient moves their cursor to the filled target as quickly as possible and holds their cursor inside the target for 1 second to end the trial. Figure 1 illustrates the flow of this task over time, with a snapshot of each stage as seen by the patient.

Patients viewed task objects on an OR monitor positioned in front of them and controlled their cursor using a Wacom Intuos pen and tablet. The task was implemented in MonkeyLogic, a MATLAB-based software that allowed for control of task flow and automatic tracking of the cursor's position, sampled at 1 kHz (Hwang et al., 2019).

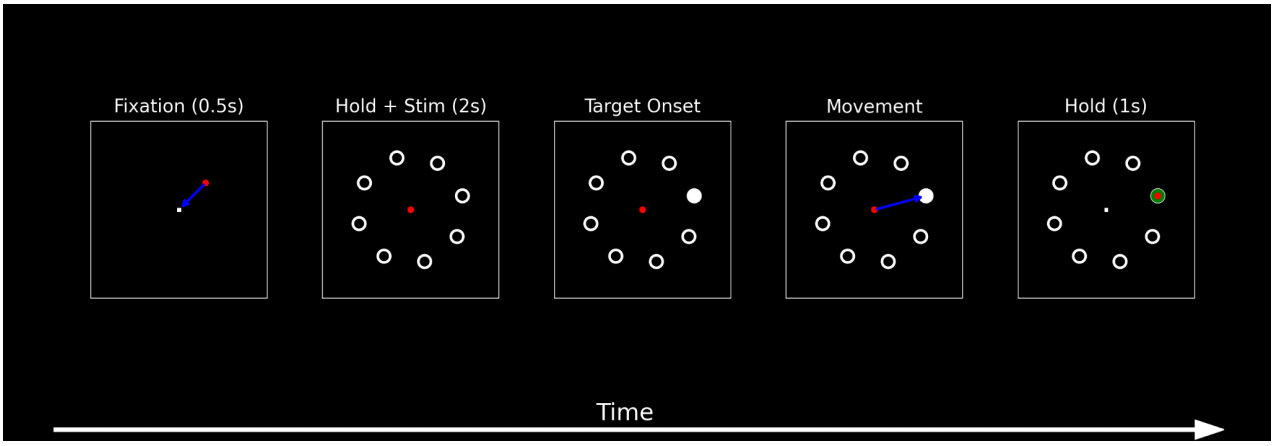

Figure 1. *Task Structure and Visual Display Across Trial Stages*.
From left to right, the squares depict the sequence of events for a single trial of the center-out reaching task used in this study. The patient begins by moving their cursor (red dot) to a central fixation point (white square), holding this position for 500 ms (Fixation). This triggers the appearance of 8 unfilled peripheral targets arranged 15° counterclockwise from the cardinal directions. The patient maintains fixation for 2 seconds during this stage, receiving continuous macroelectrode stimulation for the first 1.5 seconds (Hold + Stim). Next, one target becomes filled (Target Onset), prompting the patient to move the cursor to the filled target (Movement) and hold it within the target for 1 second (Hold). The filled target turns green upon successful completion of a trial.

Bayesian Optimization

Bayesian optimization was used to iteratively select stimulation parameters, frequency and pulse-width, which were likely to result in decreased beta power. The overall optimization procedure was divided into three distinct stages: surface mapping, optimization, and validation.

In the surface mapping stage, an initial grid search was conducted using predefined proportions (10%, 50%, and 90%) of the safe parameter ranges for frequency (40–151 Hz) and pulse width (60–120 μs). Amplitude and electrode contact were held constant throughout the

experiment – default values were 2V and contact 0 respectively, though we modified each based on the overall tolerability results of clinical stimulation. This generated nine parameter permutations, tested systematically to generate a "prior" map of energy values in the frequency vs. pulse-width parameter space, to inform the optimization algorithm. Parameters were constrained within safe bounds to ensure patient safety.

The optimization stage involved further development of the prior as well as the Bayesian optimization method itself. During the first stage of optimization, Sobol sequences were generated (using SciPy Sobol) to explore the parameter space efficiently and develop a more detailed prior. Sobol sequences are quasi-random, low-discrepancy sequences that fill the space more uniformly than random sampling. For a space in j dimensions, a Sobol sequence of length i can be generated recursively, with the jth component of the ith point defined by:

$$x_{i,j} \coloneqq i_1 v_{1,j} \oplus i_2 v_{2,j} \oplus \cdots,$$

where $v_{k,j}$ is the kth of a set of precomputed direction numbers for dimension j, i_k is the kth digit in the binary expression of i, and $\oplus$ is the bitwise exclusive OR (XOR) operation (Joe & Kuo, 2008). We generated a 2-dimensional Sobol sequence corresponding to points in the 2-dimensional frequency vs. pulse-width parameter space, allowing for pseudorandom exploration of stimulation effectiveness. Figure 2 shows a visualization of the parameter sets that were ultimately tested after Sobol sequence generation.

Figure 2. *Sobol Sequence-Generated Parameter Sets for Initial Optimization Stage*
Visualization of the stimulation parameter sets tested during the first stage of optimization, generated using a 2-dimension Sobol sequence of length 11. Each red square represents a unique trial, plotted based on its location in the frequency vs. pulse-width space. Only 8 parameter sets were tested (rather than all 11 generated) because 3 trials were replaced with random no-stimulation baseline activity recordings.

In the second stage of optimization, we implemented a Gaussian Process Regression (GPR), using scikit-learn GaussianProcessRegressor, to model the unknown relationship between stimulation parameters and beta. In Bayesian optimization, the GPR serves as a surrogate model – rather than testing every combination of parameters, we use the GPR to predict beta for untested parameters, given a prior of previously tested values. The GPR treats the unknown function as a distribution over functions, where the finite set of tested points follows a

multivariate Gaussian distribution (Rasmussen & Williams, 2008). For a set of input points $X = \{x_1, \cdots, x_n\}$ with observed values y, the GPR's prediction y_* at a new point x_* is normally distributed:

$$y_* \sim N(\mu(x_*), \sigma^2(x_*),$$

where:

- the predicted mean (expected beta power) is $\mu(x_*) = k(x_*, X)^T [K + \sigma_n^2 I]^{-1} y$
- the standard deviation is $\sigma^2(x_*) = k(x_*, x_*) - k(x_*, X)^T [K + \sigma_n^2 I]^{-1} k(x_*, X)$

Here, $k(x, x')$ is the radial basis function kernel, K is the covariance matrix of prior tested points, and $\sigma_n^2 I$ is a noise term added for regularization.

The estimates for untested points stored in the GPR are then used to choose the next set of parameters for testing through maximization of an acquisition function, which balances exploitation (sampling where the mean prediction is low) and exploration (sampling where uncertainty is high). We used the Probability of Improvement (PI) acquisition function, defined as:

$$PI(x) = \Phi(f_0; \mu(x), K(x, x)),$$

where f_0 is the minimum value observed so far and Φ denotes the cumulative distribution function (CDF) of the normal distribution with mean $\mu(x)$ and variance $K(x, x)$ (Garnett, 2015). Each chosen parameter permutation was then evaluated by stimulating the patient, simultaneously recording the LFP during stimulation, and calculating normalized beta-band power from the periodogram of the artifact-rejected signal (generated using SciPy Welch with no sliding window).

Following optimization, we used a validation stage to ensure robustness in the results of optimization. The optimized parameter set was compared to a selection of random permutations and previously-tested configurations, to confirm that it consistently resulted in lower beta and was not likely to be a local minimum of the GPR model. Testing randomized conditions also helped in assessing the generalizability and reliability of optimization.

Throughout the experiment, baseline recordings were collected at both regular and random intervals to monitor changes in non-stim beta power and ensure the reliability of comparisons between stimulation parameters. Three "baseline checks" each were conducted at the start and end of the experiment, in addition to random checks throughout the optimization stage. All recorded data, including LFPs, parameter configurations, and energy values, were stored in pickle files organized by trial for further analysis.

Artifact Rejection

To reduce the effect of stimulation artifacts on beta power calculation, an artifact rejection algorithm based on phase portrait analysis was developed and applied. The algorithm takes advantage of the artifact's significant deviations from baseline activity in terms of voltage (V) and its derivative, velocity (dV/dt). In the phase space defined by V and dV/dt, real neural activity is expected to be tightly clustered around a mean of 0 in both dimensions, as opposed to artifact, which has significantly larger amplitude and/or velocity values even at our sampling rate of 44 kHz. Clustering methods were therefore used to identify the real neural activity points, enabling removal of the non-cluster artifact points from the signal.

The algorithm begins with an estimation of the stimulation period based on the mean of interpeak intervals, followed by segmentation of the LFP signal into discrete time windows

corresponding to cycles of stimulation. For each segment, DBSCAN (epsilon = 0.2, minPts = 0.5% of segment) is applied to a 2D representation of the data in the phase space. This allows for labeling of real neural activity by finding the lowest variance cluster that constitutes at least 40% of the segment. After identifying the artifact-free cluster for each segment, the entire signal is reconstructed with a linear mean interpolation between adjacent segments to preserve smooth transitions and original signal length. Figure 3 shows an example of the algorithm's performance on a raw neural recording.

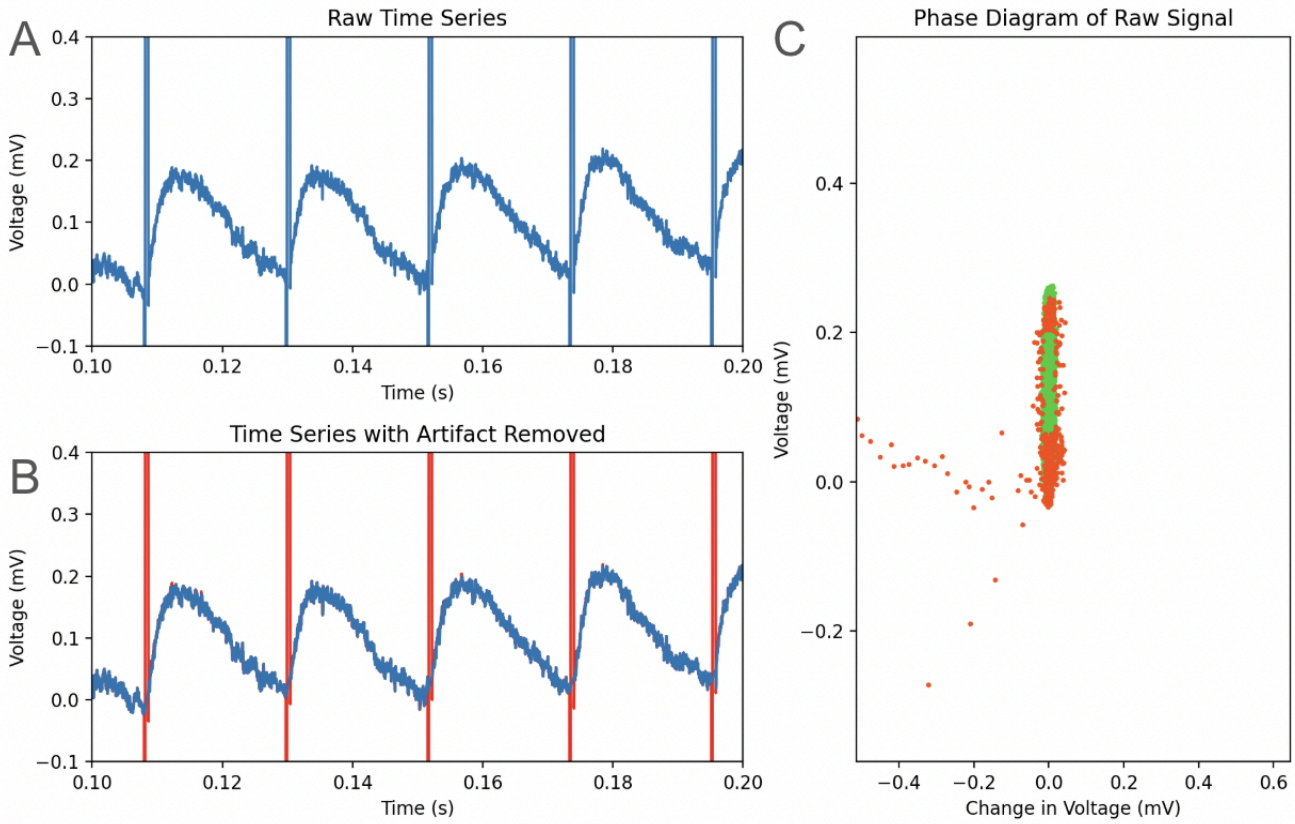

Figure 3. *DBSCAN-based Artifact Rejection Applied to a Stimulation LFP.*
(A) Raw neural recording with stimulation artifacts, zoomed in to see baseline activity. (B) DBSCAN-based artifact rejection applied to the signal in panel A. The clean signal is blue, with red indicating rejected artifact points from the original recording. (C) Cumulative voltage vs. velocity phase portrait for all segments of the raw signal, zoomed in to the clustered region. Points labeled as artifact are red, and real neural activity is green.

Experimental Flow

The flow of the experiment is controlled through the patient's behavior, with information being relayed between intraoperative devices as shown in Figure 4. The instructed-delay center out task that engages the patient is continuously run through MonkeyLogic on the behavioral computer (BHV), meaning that BHV serves as the source of instruction for all other devices throughout the experiment. Upon initiation of the Hold + Stim stage of the behavioral task, BHV automatically sends a behavioral code via PCIe to a data acquisition device (DAQ). The DAQ then relays the behavioral codes through a signal splitter box to Port-1 of both left and right Neuro Omega devices simultaneously. Throughout this time, the closed-loop computer (CL) is running the Bayesian optimization python file (stim_design.py) through the terminal. Between experimental trials, stim_design.py instructs CL to continuously stream behavioral codes via an Ethernet cord that is connected to the Neuro Omega device contralateral to the patient's dominant hand. When BHV sends a particular behavioral code to Port-1 of the Neuro Omegas, CL almost instantly receives that code and instructs the Ethernet-connected Neuro Omega accordingly. If the code sent by BHV indicates a baseline trial, CL will initiate 1.5s of no-stim recording. On the other hand, a stimulation code sent by BHV will cause CL to instruct the connected Neuro Omega to stimulate the patient for 1.5s, with parameters specified by the optimization in stim_design.py. Whether a stimulation or baseline trial, CL will complete its instruction of the Neuro Omega, record the LFP signal, calculate beta power, save the trial's data, and prepare to receive the next behavioral code from MonkeyLogic through the Neuro Omega.

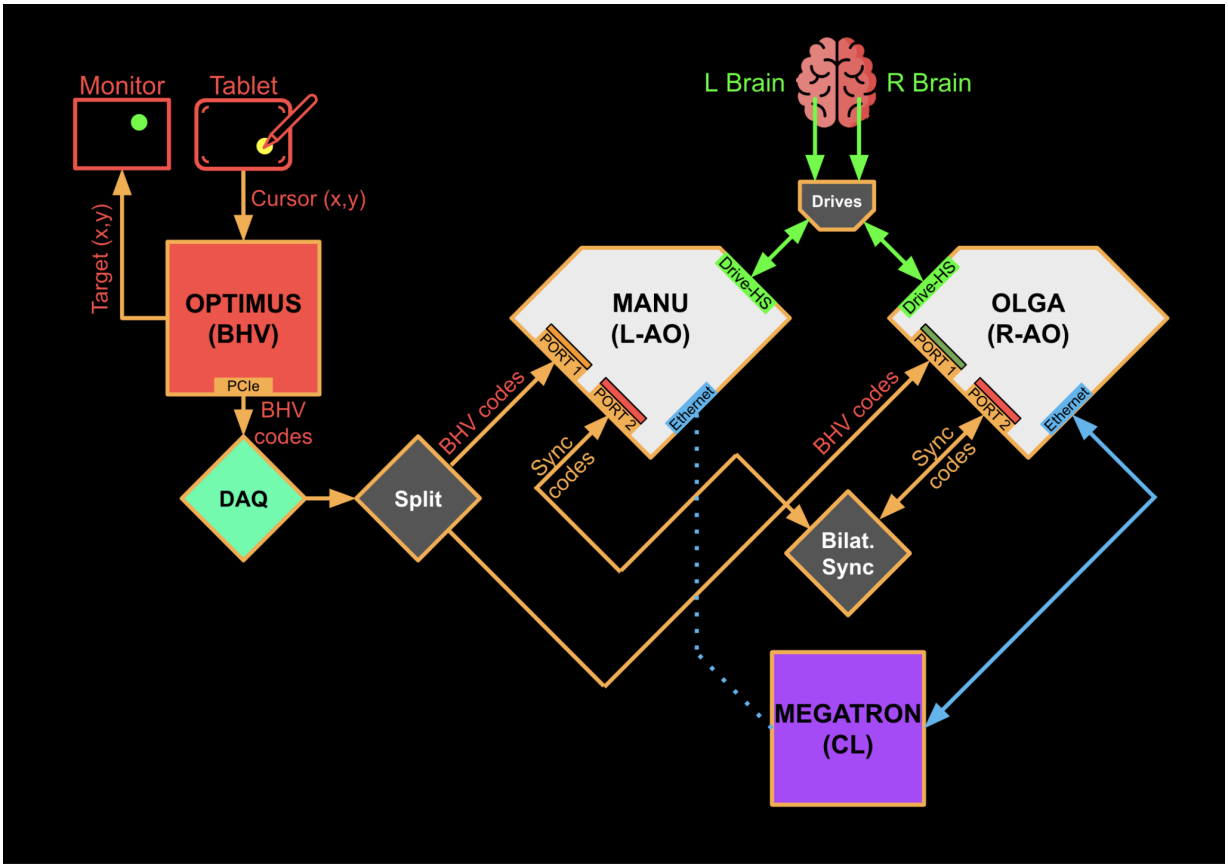

Figure 4. *Schematic of Experimental Hardware and Data Communication*.
The behavioral computer (OPTIMUS/BHV) controls the task through MonkeyLogic, displaying task objects on an OR monitor and receiving patient cursor input from a touchscreen tablet. Behavioral codes are transmitted via PCIe to a data acquisition device (DAQ), which forwards them to a splitter that simultaneously routes the codes to both Neuro Omega systems (MANU for left brain hemisphere, OLGA for right). The closed-loop computer (MEGATRON/CL) interfaces with a Neuro Omega through Ethernet, streaming behavioral codes and performing stimulation/analysis as instructed by the behavioral codes. Bilateral synchronization simultaneously sends a series of codes to both Neuro Omegas throughout the experiment, which are used to align the data post-hoc. Figure created by Sid Udata.

Results

The primary objective of this study was to evaluate the effectiveness of Bayesian optimization in minimizing beta power through systematic parameter selection and testing. Additionally, we sought to investigate whether reductions in beta power correlated with improved motor performance on our modified reaching task. By integrating real-time neural recordings with adaptive stimulation, this study aimed to validate Bayesian optimization as a potential method for automated parameter selection in closed-loop DBS for Parkinson's Disease.

Parameter Optimization

A total of 83 experimental trials, each including LFP data and behavioral data, were recorded from one patient and used for further analysis. To assess the effect of Bayesian optimization on beta power reduction, we analyzed the distribution of beta across all experimental trials. Figure 5 shows the evolution of normalized beta power throughout the different experimental conditions, namely baseline/non-stim recordings, surface mapping, optimization, and validation.

Baseline recordings established a reference level of beta in the absence of stimulation, with a mean of 0.14 and range from 0.07 to 0.23. This large range indicates that the behavioral task did not stabilize baseline beta as well as expected for this subject, suggesting variability in the patient's neural state; additional testing on more patients is needed to determine whether this trend persists and whether a redesigned task is necessary. In contrast to baseline recordings, stimulation trials showed much lower beta values, with a mean of $4x10^{-4}$ and range from $6x10^{-5}$ to $3x10^{-3}$. This stark difference in the scale of beta measurements between baseline and stimulation trials can be attributed in part to the beneficial effects of stimulation, though it is also

impacted by imperfect artifact rejection that leaves residual spectral power at the stimulation frequency and its harmonics.

Variations in beta power across trial conditions (mapping, opt1/Sobol optimization, opt2/GPR optimization, validation) reflect the importance of parameter optimization, as different combinations of frequency and pulse-width resulted in vastly different effects on beta oscillations. Upward and downward fluctuations in beta during optimization, as opposed to a monotonically downward trend, reflect the Bayesian optimization algorithm's competing goals of exploring the parameter space and targeting regions most likely to contain the global minimum. That said, the last 10 trials of opt2/GPR optimization demonstrate the expected downward trend. In fact, all of the stimulation trials from 66–71 used the same stimulation parameters (46 Hz, 115 μs), likely because the algorithm converged on the minimum. The observation that these equal-parameter trials all had similar levels of beta is also promising, as it demonstrates the reliability of each parameter set's effect on LFP activity.

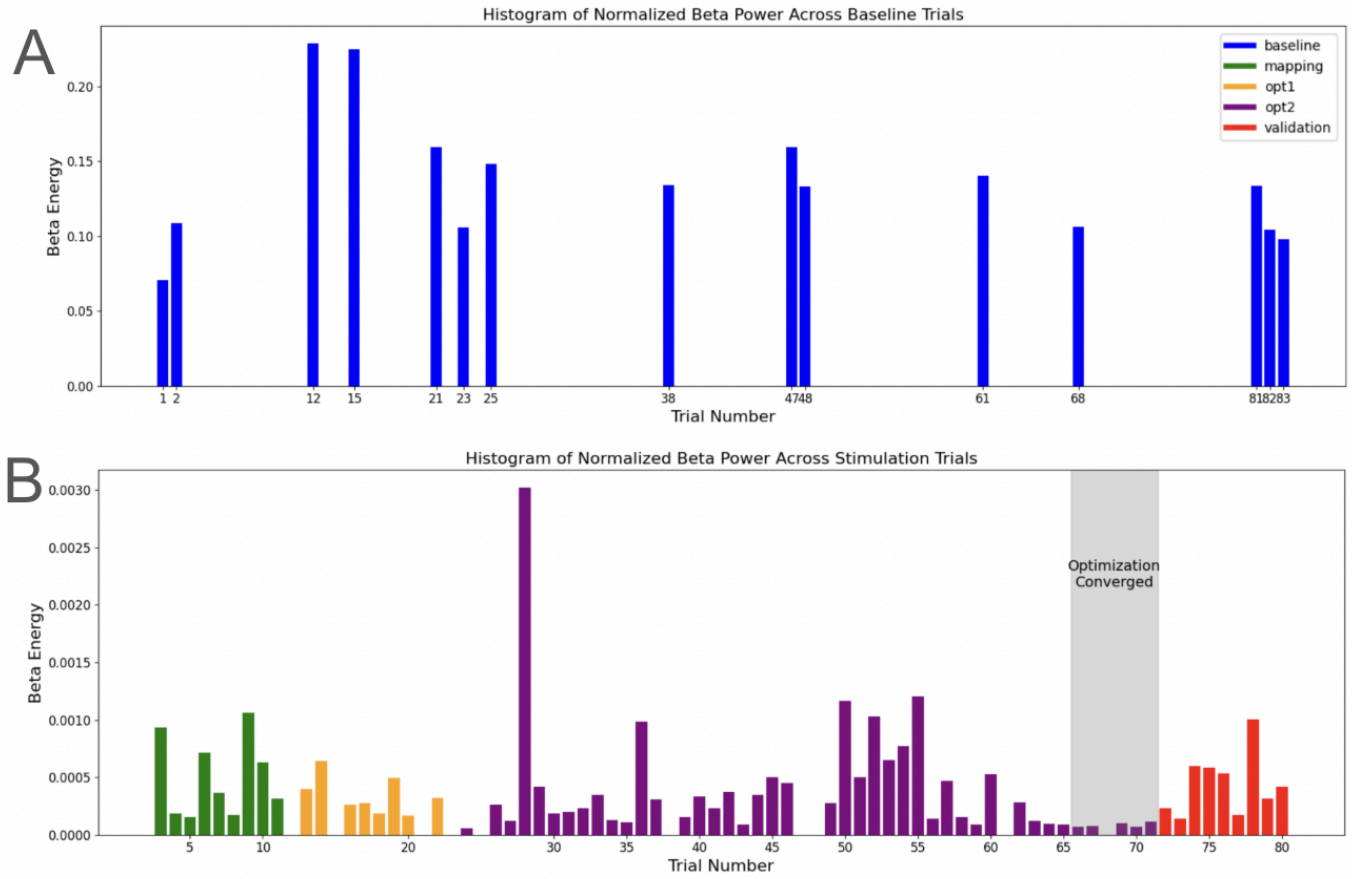

Figure 5. *Normalized Beta Power Across Trials*
Overview of beta energy values from each trial, color-coded by condition: baseline/non-stim (blue), surface mapping (green), Sobol sequence optimization (opt1, yellow), Gaussian Process Regression optimization (opt2, purple), and validation (red). Axes are rescaled for ease of comparison between (A) baseline trials and (B) stimulation trials.

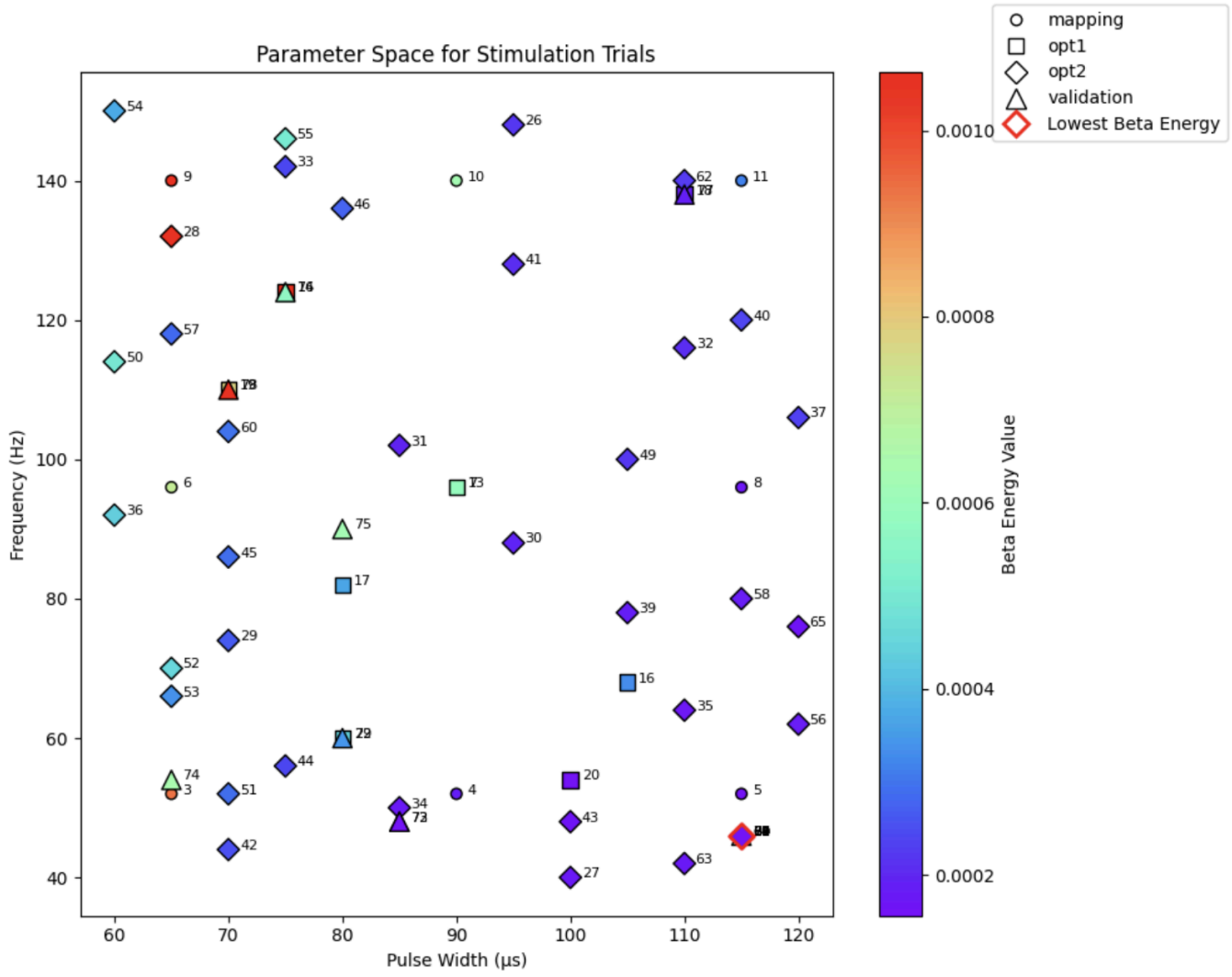

Figure 6. *Beta Power as a Function of Stimulation Parameters Across Trials*
Each stimulation trial of this experiment is represented by a marker corresponding to the stimulation's frequency and pulse width, though some trials overlap due to repeated testing of specific parameter sets. Marker color corresponds to the trial's recorded beta energy, with cooler colors reflecting lower beta. Trial numbers and marker shapes indicating the experimental stage provide a temporal sense of the sequence of parameter exploration. The trial yielding the minimum beta energy is highlighted with a red border.

Figure 6 provides a 2-dimensional view of the stimulation parameter sets and beta values observed throughout the experiment. Each trial is represented at the applied stimulation's location in the frequency vs. pulse-width parameter space, with the marker shape corresponding to experimental stage and marker color indicating beta power. Trial numbers are labeled to give a

sense of how the parameter space was explored over the course of the experiment, and the parameter set with minimum beta power value is highlighted with a red border.

Initial parameter exploration during the surface mapping stage and first portion of optimization covered a broad range of parameter sets to generate an informative prior for the Bayesian optimization algorithm. As optimization progressed, however, tested stimulation parameters became more concentrated in the low frequency, high pulse-width region of the parameter space. Specifically, the 40–90 Hz frequency range and 100-120 μs pulse width range showed consistently low relative beta and was therefore explored repeatedly at the end of optimization. Although no meaningful conclusions can be drawn from this plot alone, given that it was generated from only one patient, the consistency of low beta power under 90 Hz is interesting given that clinical DBS is typically conducted at 130 Hz or greater (Kuncel & Grill, 2004).

Motor Performance

While beta power reduction is the target of our Bayesian optimization algorithm, the ultimate goal of treatment with DBS is to improve patients' symptoms. As such, we analyzed the relationship between beta power and motor performance in our center-out reaching task, to evaluate the clinical significance of optimizing stimulation parameters.

Figure 7 shows an example of the patient's cursor trajectory across the tablet for a single trial (Trial 11). This trial's movement pattern demonstrates successful task engagement and effective motor performance, as the patient smoothly transitioned from the fixation point to the correct target with minimal tremor interference. In order to quantify motor performance and discover relationships between beta and movement for each trial, we calculated several

movement metrics including reaction time, target acquisition time, and cursor velocity. Reaction time – the time elapsed between filled target onset and the start of cursor movement – was calculated as shown in Figure 8. The patient's average reaction time was 0.70 ± 0.52 seconds, and reaction time showed no significant correlation to beta energy during the pre-movement stage ($p=0.64$). We also analyzed target acquisition time – the time elapsed between filled target onset and acquisition – which had a mean of 1.58 ± 0.69 seconds but also showed no significant correlation to beta ($p=0.84$). Finally, we analyzed both average and peak cursor velocity during the movement period. Average velocity had a mean of 2.34 ± 0.33 degrees of visual angle per second and was positively correlated with beta, though the relationship was not significant ($p=0.075$). Peak velocity, which had a mean of 217.81 ± 52.87 degrees of visual angle per second, had a positive correlation with beta as well, but this relationship was moderately significant ($p=0.016$). Progressive fatigue throughout the experiment was considered as a confounding variable, potentially affecting motor performance independent of stimulation effectiveness, but this patient showed no significant change in movement duration ($p=0.99$) or reaction time ($p=0.22$) as the experiment progressed.

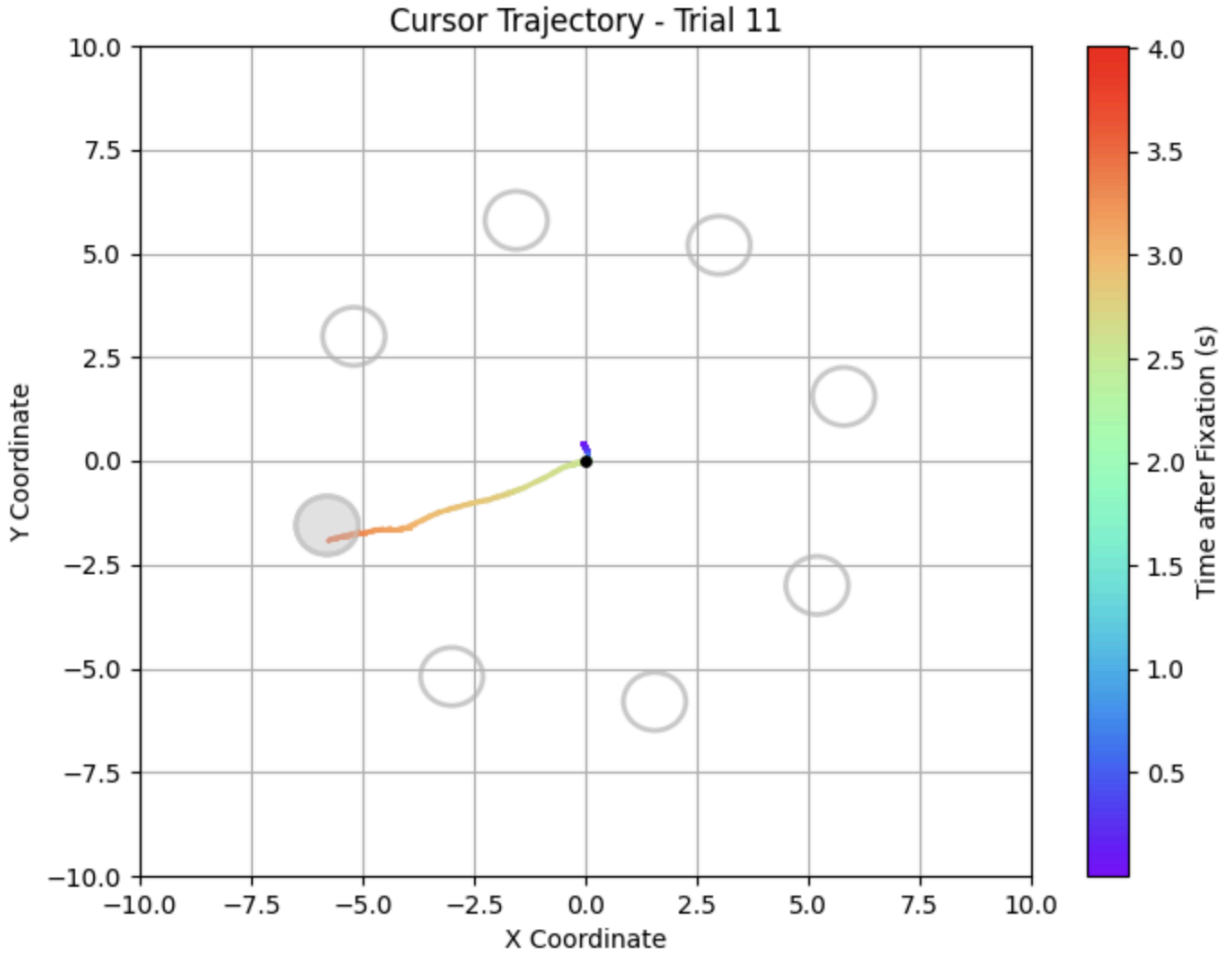

Figure 7. *Example Cursor Trajectory for a Single Trial*
Gray circles represent the locations of the task targets in the tablet's x-y coordinate system, with the filled-in circle indicating the correct target that the patient was instructed to move their cursor to. Time elapsed after fixation is indicated by the color of the trajectory at every point, with cooler colors corresponding to earlier in the trial. The trial began with the patient moving their cursor to the central fixation point (black dot) and maintaining fixation within a small radius of the central point. The filled-in correct target appeared 2 seconds post-fixation in every trial, though the yellow color of the trajectory as it moves away from the center indicates that the patient only started moving at 3 seconds post-fixation in this trial.

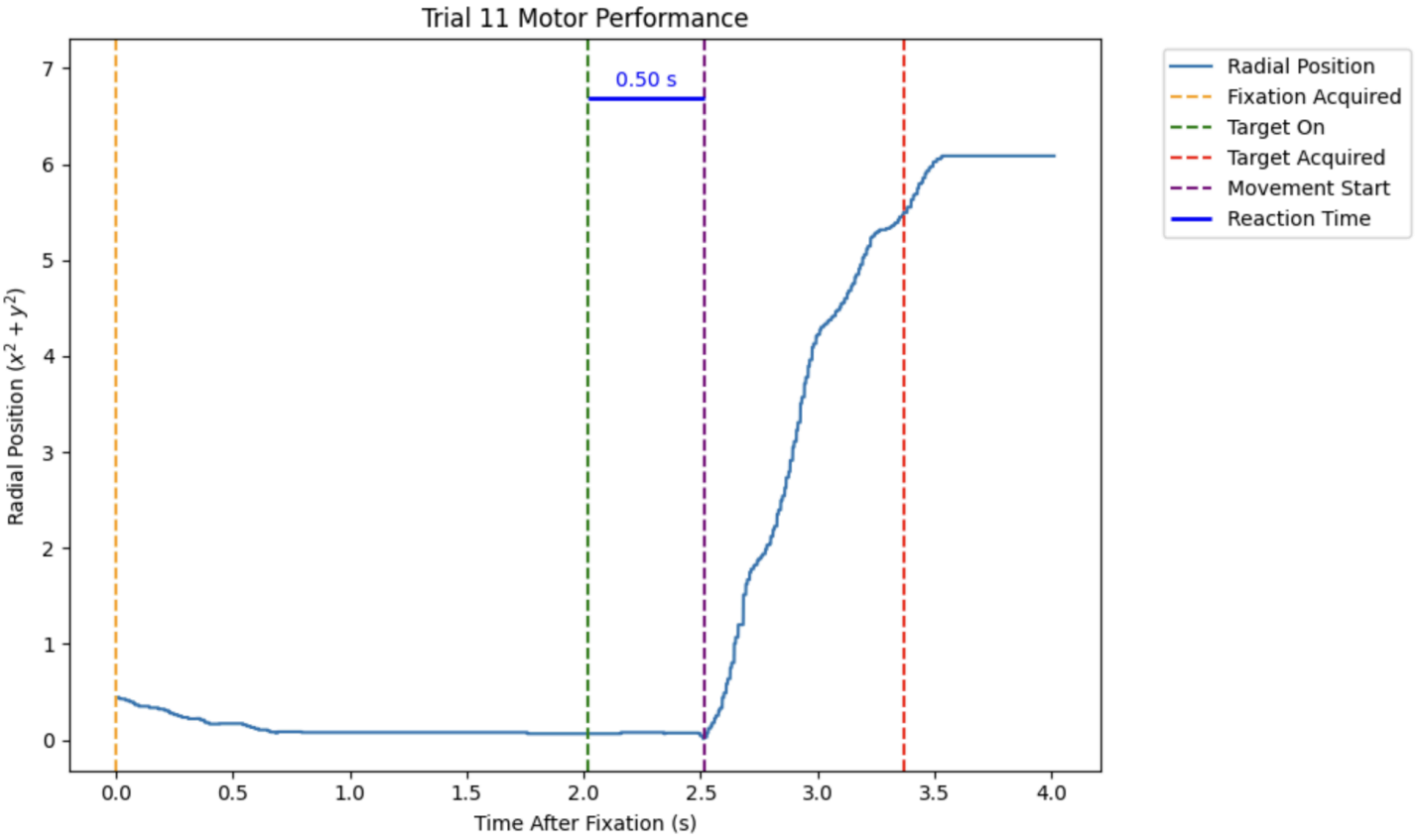

Figure 8. *Example Calculation of Reaction Time for a Single Trial*
Radial position of the cursor ($\sqrt{(x^2 + y^2)}$) is plotted as a function of time following fixation. Key task events are marked with dashed lines: fixation acquired (orange), target onset (green), and target acquisition (red). Reaction time – defined as the time between target onset and cursor movement start – is highlighted in blue and calculated as 0.50 seconds for this trial.

Artifact Rejection Limitations

A major limitation of this study, which biased the calculation of beta throughout the experiment and likely impacted the statistical significance of results, was incomplete artifact rejection. Although the DBSCAN algorithm improved the quality of most recorded LFPs by removing stimulation artifacts, there were a significant number of trials in which the algorithm rejected real data and/or left artifact points in the cleaned signal. Rejected neural activity resulted in inaccurate power spectrum measurements, and un-rejected artifact points left residual energy at the stimulation frequency and its harmonics. We noted that the algorithm performed

particularly poorly on signals longer than 1 second, in part due to low-frequency oscillations that result in a shift in the neural activity baseline. In order to improve the accuracy of beta power calculations for parameter optimization, we sought to create a new algorithm that more accurately and efficiently removes artifacts from recorded LFPs, in a way that is robust to variations in signal length and amplitude of baseline activity.

Several artifact removal strategies were considered, including template subtraction methods similar to those found in the literature (Qian et al., 2017; Dastin-van Rijn et al., 2021). Template subtraction is a technique that involves generating an average artifact "template" and subtracting it periodically from each instance of stimulation in the raw signal. Assuming linear superposition of stimulation and neural activity, this subtraction method has the potential to completely recover original neural activity as it would have been recorded without any stimulation. That said, template subtraction faces a challenge in that it is very sensitive to temporal misalignment. Because stimulation artifacts are several orders of magnitude larger than neural signals, any offset between the template and an artifact can result in large distortions and the introduction of new artifacts to the signal. Moreover, template-based methods are not well-suited to our experimental setup, in which frequent stimulation parameter changes would necessitate generation of a new template each trial.

Trailing Box Artifact Rejection

To address the limitations of our original artifact rejection algorithm and improve accuracy in beta power calculations, we developed a new "trailing box" approach. Building on the principle of clustering in the voltage vs. velocity phase space, we define a rectangular "box" in the phase portrait that serves as a decision boundary between neural and stimulation activity.

However, rather than re-clustering every stimulation cycle, the center of the box updates with each successive data point based on a trailing average of the most recent neural activity. The dynamic nature of this approach allows for accommodation of low-frequency changes in the signal baseline, improving robustness while preserving high computational efficiency. Figure 9 demonstrates an example of the problem of baseline drift as well as the trailing box method's solution.

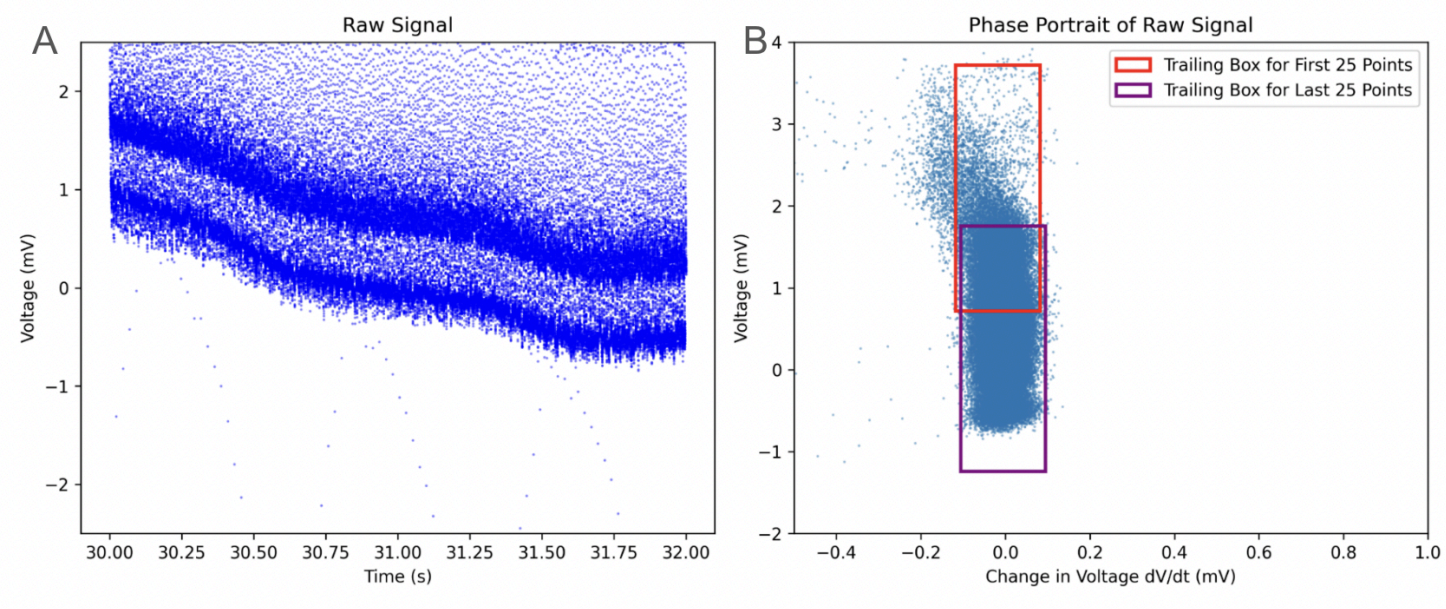

Figure 9. *Illustration of Low-Frequency Baseline Drift and Trailing Box Solution*
This figure represents recorded LFP data during stimulation in (A) the time domain and in (B) the voltage vs. velocity phase space. The raw signal demonstrates a low-frequency downward shift in the baseline of neural activity, which presents a challenge for template- and DBSCAN-based artifact rejection methods. The trailing box method accounts for baseline shifts as seen in (B), where the central cluster of real points has shifted down significantly by the end of the signal to account for the downward movement.

The trailing box algorithm proceeds as follows. The signal is first bandpass filtered from 300–9000 Hz to flatten the baseline signal for easier artifact identification. Then, each point is evaluated one by one to see if it falls within the "box" of thresholds: ±1.5 mV in voltage and ±0.1 mV in velocity. The center of the box is updated based on an exponential moving average of

the most recent 25 data points, to adjust for changes in the baseline of the signal. The indices within the signal that are considered artifact are saved and, once the entire signal has been checked, the corresponding indices of the original unfiltered signal are replaced by white noise so as not to influence the power spectrum. Random noise points are generated by pulling from a normal distribution with mean equal to the instantaneous amplitude center of the box, and standard deviation equal to that of the last 25 points. The algorithm results in a clean signal that is the same as the original signal, with artifact points replaced by random noise.

To assess the effectiveness of our algorithm, we first tested trailing box artifact rejection on semi-synthetic data. As opposed to real stimulation LFP data, in which there is no "ground truth" of the signal without stimulation, semi-synthetic data analysis allows for periodic addition of an artifact to a known, real baseline LFP and comparison of the artifact-rejected signal to that baseline. Figure 10 shows the trailing box's performance on semi-synthetic data—the clean signal preserves both low- and high-frequency oscillatory activity of the original baseline recording. Additionally, the power spectrum of the clean signal closely matches that of the original baseline, with an MSE of 1.45×10^{-14}. These results demonstrate that the trailing box method can effectively remove complex artifacts while preserving temporal and spectral characteristics of the original neural signal.

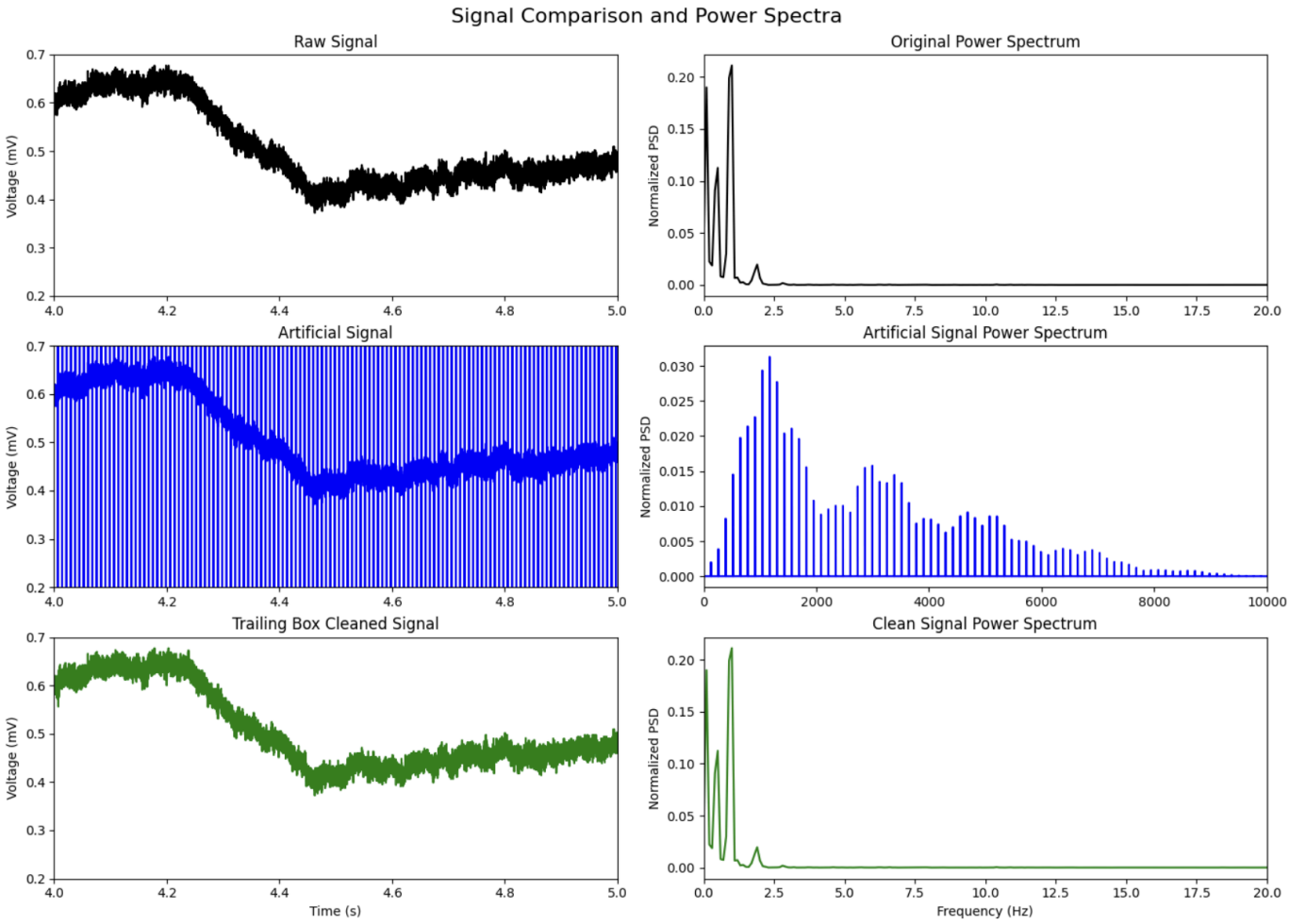

Figure 10. *Evaluation of Trailing Box Artifact Rejection on Semi-Synthetic Data*
Top row: (Left) A raw LFP signal with no stimulation, recorded during a baseline/non-stim trial. (Right) Power spectrum of the baseline neural signal
Middle row: (Left) Semi-synthetic signal, with artifact shape added linearly at 130 Hz. (Right) Power spectrum of the semi-synthetic signal, with dominant harmonic components due to artifact addition.
Bottom row: (Left) Output signal resulting from artifact rejection applied to the semi-synthetic signal. (Right) Power spectrum of the artifact-rejected clean signal

When applied to real neural data, the trailing box algorithm demonstrated superior performance to the DBSCAN approach. Figure 11 shows a comparison between raw neural data recorded during parameter optimization and the cleaned signals produced by both artifact rejection algorithms. Even though no baseline shift is evident, due to the short timescale depicted, the trailing box algorithm has a clear advantage over the DBSCAN-based method in its

ability to capture physiological activity and avoid residual artifacts. Critically, this improvement also translated to the frequency domain. While both methods effectively suppress energy at harmonics of the stimulation frequency (96 Hz in this case) compared to the original signal, the trailing box algorithm demonstrates fewer harmonic peaks in its power spectrum. As such, beta calculations from signals cleaned with the trailing box algorithm were on average 75% greater than those cleaned with clustering, reflecting a greater unmasking of real physiological activity.

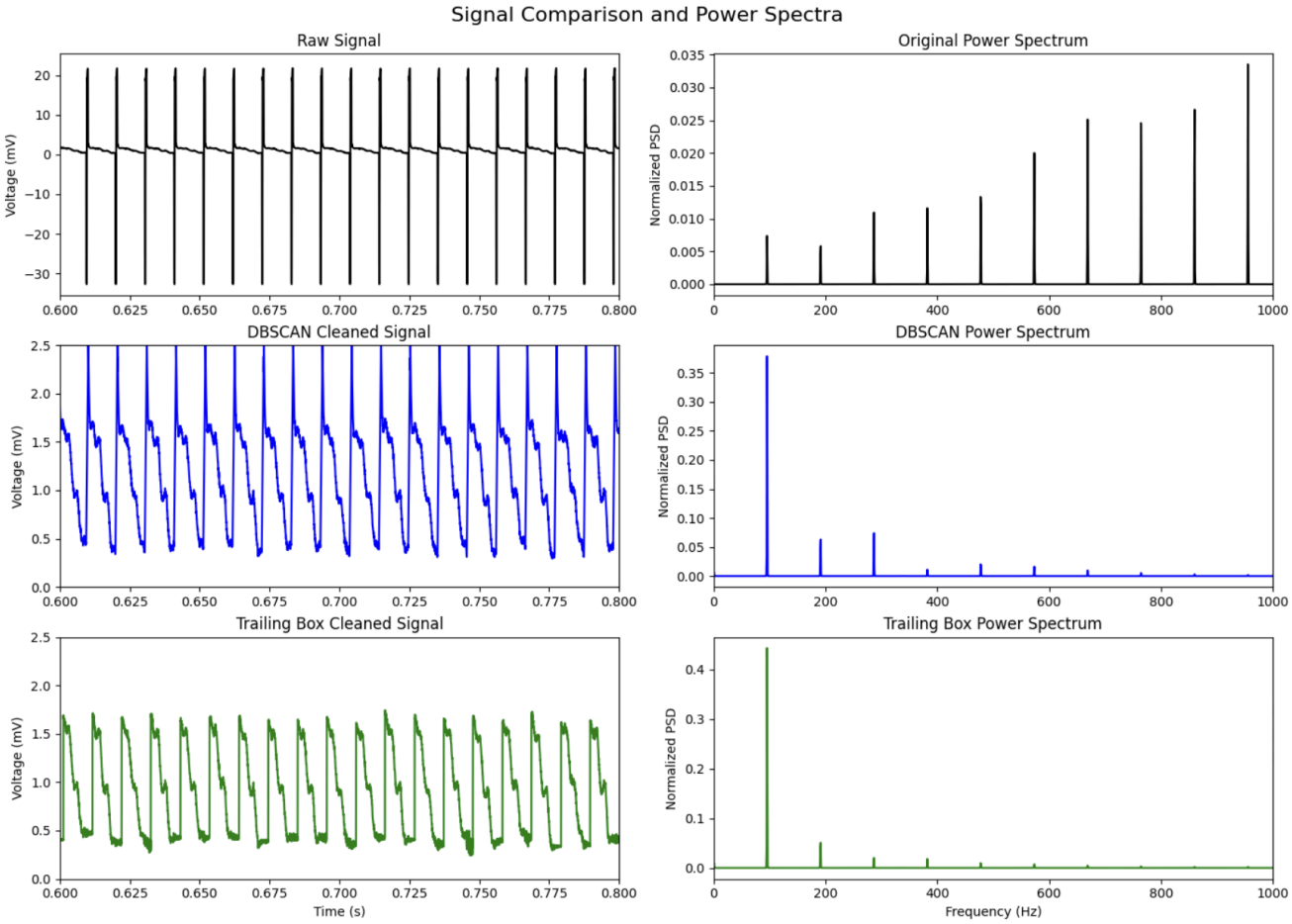

Figure 11. *Evaluation of Trailing Box Artifact Rejection on Real Neural Data*
Top row: (Left) A raw LFP signal with stimulation, recorded during a stimulation trial. (Right) Power spectrum of the baseline neural signal
Middle row: (Left) Output signal resulting from DBSCAN-based artifact rejection applied to the raw signal. (Right) Power spectrum of the DBSCAN-cleaned signal
Bottom row: (Left) Output signal resulting from trailing box-based artifact rejection applied to the raw signal. (Right) Power spectrum of the trailing box-cleaned signal

Discussion and Future Directions

Significance of Findings

This study presents a novel application of Bayesian optimization to Parkinson's disease DBS parameter selection, using behavior to control the patient's neural state and optimizing in the 2-dimensional frequency vs. pulse-width parameter space. Using a closed-loop neuromodulation paradigm, our system integrated stimulation testing with real-time neural feedback and successfully converged on a low-beta region of the parameter space. These findings demonstrate the feasibility of using closed-loop approaches with data-driven algorithms to automate DBS parameter tuning, offering a promising alternative to manual programming.

The implementation of a novel artifact rejection algorithm was also a key advancement, improving the reliability of beta power estimation. This method preserves temporal and spectral characteristics of the signal with high fidelity, enabling more accurate real-time measurement of beta and other neural biomarkers. Given that stimulation artifacts are a major barrier to effective closed-loop DBS, improvements in artifact rejection are essential to implementing adaptive neuromodulation in a clinical setting.

Our observation that a low-frequency, high pulse-width parameter set yielded the greatest beta suppression is consistent with emerging literature demonstrating that non-canonical stimulation settings can provide therapeutic benefits for some individuals (Conway et al., 2021; Vijaratnam et al., 2021). While clinical DBS is typically delivered at high frequencies (>130 Hz), our results support growing evidence that low frequency stimulation may yield equal or better outcomes, especially when guided by real-time neural data and patient-specific tuning.

Future Directions

Despite demonstrating promising results, the current study is limited by its small sample size. Although we observed slight trends in the relationship between motor performance metrics and beta, the data was insufficient to reach statistical significance. Different subjects are also likely to exhibit different trends, which means that finding more rigorous cross-subject correlations will require an increased sample size. One imminent solution to promote patient involvement in neuromodulation studies is the use of externalized leads and postoperative testing (Kashanian et al., 2021). In contrast to intraoperative experiments, which face significant constraints due to limited time and patient fatigue, externalized leads allow for greater flexibility and more robust data collection outside of the operating room.

Several changes should also be made to the current experimental paradigm, to improve the significance of results. For example, as seen in Figures 5 and 6, the validation stage featured many stimulation trials that resulted in high beta. This occurred due to the random nature of validation testing, which allowed for unnecessary tests in regions of the parameter space known to have higher beta values. A more efficient validation scheme would focus testing on the more promising, low-beta region of the parameter space. Our experiment could also be improved by incorporating stimulation during movement, to allow for more accurate movement-beta relationships. Currently, stimulation is only delivered during the pre-movement stage, limiting the results by not accounting for the dynamic nature of beta following stimulation. A redesigned experiment incorporating stimulation/recording both before and during movement could better capture the full trajectory of beta-related motor dysfunction and more effectively evaluate the impact of stimulation on behavior.

Future studies might also build on this work by exploring optimization of other stimulation parameters such as amplitude and contact. These parameters may interact with frequency and pulse-width in patient-specific ways, and higher-dimensional optimization has the potential to yield more precise stimulation profiles tailored to each individual. The current study also focused only on optimizing stimulation parameters within a fixed window. However, future studies integrating parameter optimization with adaptive timing could more effectively target periods of motor dysfunction to improve symptoms while minimizing side effects.

Finally, continued development of artifact rejection algorithms remains a priority in order to reliably and accurately compare biomarker measurements across stimulation settings. Hyperparameters for the trailing box algorithm (threshold sizes and length of the trailing average) were found through trial and error, leaving room for the discovery of more optimal or signal-specific values. Further signal processing methods could also be applied to "flatten" the residual periodic nature of artifact-rejected signals, which arises from nonlinear interactions between stimulation and neural activity. Although our algorithms effectively remove power spectral density at stimulation harmonics, removing these remaining oscillations would further decrease energy at the stimulation frequency itself and allow for more accurate biomarker measurement.

References

Akbar, U., & Asaad, W. (2017). A Comprehensive Approach to Deep Brain Stimulation for Movement Disorders. Rhode Island Medical Journal.

Alpha Omega, Nazareth, Israel. "Nero Omega." https://www.alphaomega-eng.com/Neuro-Omega-System

Ballard, C., et al. (2009). The UPDRS scale as a means of identifying extrapyramidal signs in patients suffering from dementia with Lewy bodies. Acta Neurologica Scandinavica, 96(6), 366–371. https://doi.org/10.1111/j.1600-0404.1997.tb00299.x

Bouthour, W., Mégevand, P., Donoghue, J. et al. Biomarkers for closed-loop deep brain stimulation in Parkinson disease and beyond. Nat Rev Neurol 15, 343–352 (2019). https://doi.org/10.1038/s41582-019-0166-4

Buyan-Dent, L., Mangin, T., & Shannon, K. M. (2018). Pharmaceutical Treatment of Parkinson's Disease. Practical Neurology.

Chade, A. R., Kasten, M., & Tanner, C. M. (2006). Nongenetic causes of parkinson's disease. Parkinson's Disease and Related Disorders, 147–151. https://doi.org/10.1007/978-3-211-45295-0_23

Connolly, M. J., Cole, E. R., Isbaine, F., de Hemptinne, C., Starr, P. A., Willie, J. T., Gross, R. E., & Miocinovic, S. (2021). Multi-objective data-driven optimization for improving deep brain stimulation in parkinson's disease. Journal of Neural Engineering, 18(4), 046046. https://doi.org/10.1088/1741-2552/abf8ca

Conway, Z.J., et al. Low-frequency STN-DBS provides acute gait improvements in Parkinson's disease: a double-blinded randomised cross-over feasibility trial. J NeuroEngineering Rehabil 18, 125 (2021). https://doi.org/10.1186/s12984-021-00921-4

Cuschieri, A., Borg, N., & Zammit, C. (2022). Closed Loop Deep Brain stimulation: A systematic scoping review. Clinical Neurology and Neurosurgery, 223, 107516. https://doi.org/10.1016/j.clineuro.2022.107516

Dastin-van Rijn, E. M. et al. (2021). Uncovering biomarkers during therapeutic neuromodulation with Parrm: Period-based Artifact Reconstruction and Removal Method. Cell Reports Methods, 1(2), 100010. https://doi.org/10.1016/j.crmeth.2021.100010

Dorsey, E. R., Sherer, T., et al. (2018). The emerging evidence of the parkinson pandemic. Journal of Parkinson's Disease, 8(s1). https://doi.org/10.3233/jpd-181474

Gandhi, K. R., & Saadabadi, A. (2023). Levodopa (L-Dopa). StatPearls.

Garnett, R. (2015, March 16). Bayesian Optimization: Acquisition Functions. CSE 515T: Bayesian Methods in Machine Learning. https://www.cse.wustl.edu/~garnett/cse515t/spring_2015/files/lecture_notes/12.pdf

GaussianProcessRegressor. scikit-learn. (n.d.). https://scikit-learn.org/stable/modules/generated/sklearn.gaussian_process.GaussianProcessRegressor.html

Grado, L. L., Johnson, M. D., & Netoff, T. I. (2018). Bayesian adaptive dual control of deep brain stimulation in a computational model of parkinson's disease. PLOS Computational Biology, 14(12). https://doi.org/10.1371/journal.pcbi.1006606

Hwang, J., Mitz, A. R., & Murray, E. A. (2019). NIMH monkeylogic: Behavioral control and data acquisition in Matlab. Journal of Neuroscience Methods, 323, 13–21. https://doi.org/10.1016/j.jneumeth.2019.05.002

Joe, S., & Kuo, F. Y. (2008). Constructing sobol sequences with better two-dimensional projections. SIAM Journal on Scientific Computing, 30(5), 2635–2654. https://doi.org/10.1137/070709359

Hansen, C.A., Miller, D.R., Annarumma, S. et al. Levodopa-induced dyskinesia: a historical review of Parkinson's disease, dopamine, and modern advancements in research and treatment. J Neurol 269, 2892–2909 (2022). https://doi.org/10.1007/s00415-022-10963-w

Kashanian, A., Rohatgi, P., Chivukula, S., Sheth, S. A., & Pouratian, N. (2020). Deep brain electrode externalization and risk of infection: A systematic review and meta-analysis. Operative Neurosurgery, 20(2), 141–150. https://doi.org/10.1093/ons/opaa268

Kuncel, A. M., & Grill, W. M. (2004). Selection of stimulus parameters for deep brain stimulation. Clinical Neurophysiology, 115(11), 2431–2441. https://doi.org/10.1016/j.clinph.2004.05.031

Louie, K. H., Petrucci, M. N., Grado, L. L., Lu, C., Tuite, P. J., Lamperski, A. G., MacKinnon, C. D., Cooper, S. E., & Netoff, T. I. (2021). Semi-automated approaches to optimize deep brain stimulation parameters in Parkinson's disease. Journal of NeuroEngineering and Rehabilitation, 18(1). https://doi.org/10.1186/s12984-021-00873-9

Lozano, A.M., Lipsman, N., Bergman, H. et al. Deep brain stimulation: current challenges and future directions. Nat Rev Neurol 15, 148–160 (2019). https://doi.org/10.1038/s41582-018-0128-2

Panicker, N., Ge, P., Dawson, V. L., & Dawson, T. M. (2021). The cell biology of parkinson's disease. Journal of Cell Biology, 220(4). https://doi.org/10.1083/jcb.202012095

Pfeiffer, R. F. (2016). Non-motor symptoms in parkinson's disease. Parkinsonism & Related

Disorders, 22. https://doi.org/10.1016/j.parkreldis.2015.09.004

Qian, X., et al.. (2017). A method for removal of deep brain stimulation artifact from local field potentials. IEEE Transactions on Neural Systems and Rehabilitation Engineering, 25(12), 2217–2226. https://doi.org/10.1109/tnsre.2016.2613412

Qiu, J., et al. (2024). Deep learning and fmri-based pipeline for optimization of deep brain stimulation during parkinson's disease treatment: Toward rapid semi-automated stimulation optimization. IEEE Journal of Translational Engineering in Health and Medicine, 12, 589–599. https://doi.org/10.1109/jtehm.2024.3448392

Rasmussen, C. E., & Williams, C. K. I. (2006). Gaussian Processes for Machine Learning. MIT Press.

Rosin, B., et al. (2011). Closed-Loop Deep Brain Stimulation Is Superior in Ameliorating Parkinsonism. Neuron, 72(2).

Sarikhani, P., Ferleger, B., Mitchell, K., Ostrem, J., Herron, J., Mahmoudi, B., & Miocinovic, S. (2022). Automated deep brain stimulation programming with safety constraints for tremor suppression in patients with parkinson's disease and essential tremor. Journal of Neural Engineering, 19(4), 046042. https://doi.org/10.1088/1741-2552/ac86a2

Scangos, K.W., Khambhati, A.N., Daly, P.M. et al. Closed-loop neuromodulation in an individual with treatment-resistant depression. Nat Med 27, 1696–1700 (2021). https://doi.org/10.1038/s41591-021-01480-w

Shahed, J., & Jankovic, J. (2007). Motor symptoms in parkinson's disease. Handbook of Clinical Neurology, 329–342. https://doi.org/10.1016/s0072-9752(07)83013-2

Shults, C. W. (2006). Lewy bodies. Proceedings of the National Academy of Sciences, 103(6), 1661–1668. https://doi.org/10.1073/pnas.0509567103

Sobol. Sobol - SciPy v1.15.2 Manual. (n.d.). https://docs.scipy.org/doc/scipy/reference/generated/scipy.stats.qmc.Sobol.html

Sonne, J., Reddy, V., & Beato, M. R. (2024). Neuroanatomy, Substantia Nigra. StatPearls.

Tzagarakis, C., Ince, N. F., Leuthold, A. C., & Pellizzer, G. (2010). Beta-band activity during motor planning reflects response uncertainty. The Journal of Neuroscience, 30(34), 11270–11277. https://doi.org/10.1523/jneurosci.6026-09.2010

Vijiaratnam, Nirosen, et al. (2021), Long-term success of low-frequency subthalamic nucleus stimulation for Parkinson's disease depends on tremor severity and symptom duration, Brain Communications, Volume 3, Issue 3, fcab165, https://doi.org/10.1093/braincomms/fcab165

Vorwerk, J., Brock, A. A., Anderson, D. N., Rolston, J. D., & Butson, C. R. (2019). A retrospective evaluation of automated optimization of deep brain stimulation parameters. Journal of Neural Engineering, 16(6), 064002. https://doi.org/10.1088/1741-2552/ab35b1

Whitmer, D., de Solages, C., Hill, B., Yu, H., Henderson, J. M., & Bronte-Stewart, H. (2012). High frequency deep brain stimulation attenuates subthalamic and cortical rhythms in Parkinson's disease. Frontiers in Human Neuroscience, 6. https://doi.org/10.3389/fnhum.2012.00155

Willis, A. W., Roberts, E., et al. (2022). Incidence of parkinson disease in North America. Npj Parkinson's Disease, 8(1). https://doi.org/10.1038/s41531-022-00410-y

Wood-Kaczmar, A., Gandhi, S., & Wood, N. W. (2006). Understanding the molecular causes of parkinson's disease. Trends in Molecular Medicine, 12(11), 521–528. https://doi.org/10.1016/j.molmed.2006.09.007

Zhu, J., Cui, Y., Zhang, J., et al. (2024). Temporal trends in the prevalence of parkinson's disease from 1980 to 2023: A systematic review and meta-analysis. The Lancet Healthy Longevity, 5(7). https://doi.org/10.1016/s2666-7568(24)00094-1